POLITECNICO
MILANO 1863

SCUOLA DI INGEGNERIA INDUSTRIALE
E DELL'INFORMAZIONE

Executive Summary of the Thesis

Variable Impedance Control of a Surgical Robot for Spinal Surgery

Laurea Magistrale in Automation and Control Engineering - Ingegneria dell'Automazione

Author: Riccardo Monaco

Advisor: Prof. Elena De Momi

Co-advisor: Elisa Iovene

Academic year: 2021-2022

1. Introduction

Vertebral osteotomy is a surgical procedure that involves cutting and reshaping a vertebral bone, with an osteotom or a drill, to correct a spinal deformity or to improve spinal alignment (Figure 1). Due to the presence of delicate structures, such as the spinal cord and blood vessels, in the vicinity of the vertebrae, there is a high risk of patient injury during the procedure, as damaging these tissues may lead to serious complications [1]. Robotic systems can bring great benefits in these operations, such as enhancing surgeons' technical skills and preventing surgical instruments from unintentional damage [2]. However, robotic-assisted spinal procedures are currently limited to pedicle screw placement, while vertebral osteotomies are assessed only at a research level. Key factors in robotic-assisted vertebral osteotomies include the interactions between the robot, patient, and surgeon. While the robot is not fully autonomous and requires the surgeon to guide its movements, precise control of these interactions is essential to achieve the desired outcome. Numerous impedance control approaches have been studied for Human-Robot Interaction (HRI) and hands-on control, which is a method for controlling the interaction between the robot and its environment, by adjusting the robot's stiffness, damping, and inertia. A velocity-based approach is more suitable for reaching and positioning tasks [3], whereas a force-based approach is more appropriate for achieving co-manipulation accuracy or compliantness based on human intention [4]. Introducing the human force in the control loop represents an advantage, as it allows to change the robot parameters to improve system effectiveness. Several approaches exploit the electromyographic signals (EMG) from forearm muscles to estimate the user force [5]. The most recent approach is the use of Deep Neural Networks (DNNs) which can handle non-linear relationships between the EMG features and force [6].
The proposed study is focused on the development of a control strategy for Human-Robot Interaction. A new adaptive law is proposed, based on the reaction force measured on the robot end-effector and an estimate of the human force. The aim is to provide a safety measure to support the surgeon when contact is made with critical tissues and to keep a compliant behavior otherwise. The contact force is also exploited to generate a safety position command, that prevents damaging soft materials. In Figure 2, a representation of the overall system is shown.

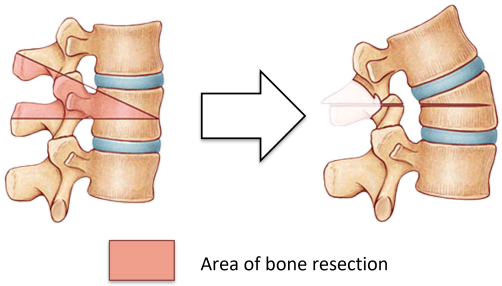

Figure 1: Example of vertebral osteotomy. On the left a side view of the spine is presented, with the area of the vertebra that requires removal indicated in red. On the right, the improvement in the spine curvature is depicted.

2. Materials and methods

2.1. Hardware components

Robotic system:
A KUKA Light-weight Robot 4+ (LWR4+) was used, which is characterized by $m = 7$ Degrees of Freedom (DOFs), position sensors on the motor sides, and joint torque sensors. The robot was controlled using Robotic Operating System (ROS) on Ubuntu 16.04, which communicated with the Fast Research Interface (FRI).

Force sensor:
The equipped force sensor was a M3815C six axis force/torque load cell (Sunrise Instruments), mounted on the seventh joint of the robot. The sensor provided a raw signal with a sampling rate of 1000 Hz which was filtered with an exponential smoothing filter, characterized by the following equation:

$$\boldsymbol{F_{filt_t}} = \alpha_f \boldsymbol{F_{raw_t}} + (1 - \alpha_f)\boldsymbol{F_{filt_{t-1}}} \qquad (1)$$

where $\boldsymbol{F_{filt}}$ and $\boldsymbol{F_{raw}}$ represents the filtered and raw force values respectively, t denotes the current time step, and α_f is the smoothing factor. The value of α_f was determined empirically and set to 0.05, resulting in a cutoff frequency of 50 Hz. To align the reference frame of the last joint with the sensor's reference frame, a rotation of $\theta_r = 20\ ^\circ$ was applied around the z-axis (Figure 3). Then, to obtain only the contribution of the interaction forces on the force sensor readings, a compensation of the tool weight was performed. Since this contribution depends on a non-linear relationship with the end effector orientation, a

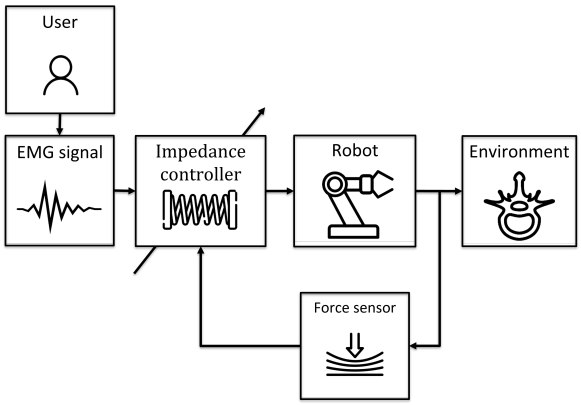

Figure 2: Scheme of the overall system: impedance parameters are adapted based on the EMG signals and the measured contact force between the robot and the environment.

MultiLayer Perceptron Regressor was trained. A dataset of 14.926 data points was collected with the robot in gravity compensation mode and divided into a training set (70%) and a testing set (30%). The training was performed using the orientation of the end effector as input and the filtered force sensor readings, $\boldsymbol{F_{filt}}$, as output. After the training, the network was able to predict the force read by the force sensor, $\boldsymbol{F_{ee}}$, without the tool's gravity contribution.

EMG sensor:
In order to measure the EMG signals coming from the human arm, the MyoWristband (Thalmic Lab) was used. The bracelet was equipped with 8 channels and communicated with a remote computer via bluetooth. The 8 EMG raw signals with a sample rate of 200 Hz were processed by the sensor itself: the absolute value of the signal was obtained with a full wave rectification and a low pass filter with 50 Hz cut-off frequency was applied to extract the envelope of the original signal. In order to extract the human force F_h, a model $\Phi : F_h = \Phi(EMG_f)$ was required. First, a dataset of approximately 14,000 data points was collected and divided into a training set (80%) and a testing set (20%). The dataset was first normalized using MinMaxScaler so that all data fell within the same range, i.e. between 0 and 1. Next, a linear regression was used to weigh the contributions of the EMG channels. Finally, an LSTM neural network was trained, using the normalized EMG sensor readings of the human forearm muscles as

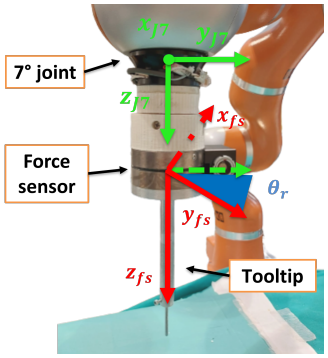

Figure 3: Representation of the calibration. In green, the reference frame of the seventh joint is shown. In red, the sensor frame of the force sensor is shown, rotated by an angle θ_r around the z-axis.

input, and the force measured by the force sensor when the user grabbed the robot from the tooltip, as output.

2.2. Control strategy

The overall control strategy is shown in Figure 4. The main control loop was represented by a Cartesian impedance controller: given as input a position setpoint, $\boldsymbol{x_{ref}} \in \mathbf{R}^n$, in the Cartesian space, with $n = 6$, a torque command $\boldsymbol{\tau_{cmd}} \in \mathbf{R}^m$ in the joint space is generated:

$$\begin{aligned}\boldsymbol{\tau}_{cmd} = \boldsymbol{J}_{pin}^{-1}(\boldsymbol{K}(\boldsymbol{x}_{ref} - \boldsymbol{x}_{curr}) + \\ + \boldsymbol{D}(\boldsymbol{D}_n, \dot{\boldsymbol{x}}_{curr})) + \boldsymbol{f}_d(\boldsymbol{q}, \dot{\boldsymbol{q}}, \ddot{\boldsymbol{q}})\end{aligned} \tag{2}$$

with $\boldsymbol{J}_{pin}^{-1} \in \mathbf{R}^{m\times n}$ the pseudo-inverse of the Jacobian matrix. $\boldsymbol{K} \in \mathbf{R}^{n\times n}$ is the Cartesian stiffness, $\boldsymbol{D_n} \in \mathbf{R}^{n\times n}$ is the Cartesian normalized damping, $\boldsymbol{x_{ref}}$ is the Cartesian reference pose, given by the difference between the position displacement imposed by the human, $\boldsymbol{x_h} \in \mathbf{R}^n$, and the additional feedback, $\boldsymbol{x_s} \in \mathbf{R}^n$. $\boldsymbol{x_{curr}} \in \mathbf{R}^n$ is the current Cartesian pose and $\boldsymbol{q}, \dot{\boldsymbol{q}}, \ddot{\boldsymbol{q}} \in \mathbf{R}^{m\times m}$ are the vectors of robot joint position, velocity, and acceleration, respectively. The Cartesian damping contribute $\boldsymbol{D}(\boldsymbol{D_n}, \dot{\boldsymbol{x}}_{\boldsymbol{curr}})$ and the inertial contribute in the joint space $\boldsymbol{f_d}(\boldsymbol{q}, \dot{\boldsymbol{q}}, \ddot{\boldsymbol{q}})$ are computed by the robot internal controller. According to the value of matrices $\boldsymbol{K}$ and $\boldsymbol{D_n}$, the robot can be more or less compliant with respect to the user's intention. The goal of this study was to develop a strategy that changed the stiffness based on both the force measured on the end-effector and the estimated force of the human. For simplicity, the strategy focused on changing the stiffness on a single axis, which is the z-axis of the seventh joint (refer to Fig. 3). The variable stiffness parameter will be denoted as $\boldsymbol{k_z}$. For the development of the control strategy, the Young's modulus of the involved tissues was considered. In particular, the Young's modulus of a cortical bone is estimated between $15 - 20\ GPa$, while for structures such as blood vessels, it is estimated in the range $2 - 6\ MPa$.

Adaptive law:
For the development of this work, the following scenario for adapting the stiffness was considered: when the robot interacted with a material with high Young's modulus (i.e. vertebra), a low $\boldsymbol{k}_z$ was maintained to ensure compliant behavior. On the other hand, when the robot interacted with a material with low Young's modulus, $\boldsymbol{k}_z$ was increased to reduce the compliantness and the risk of damaging the material. The stiffness $\boldsymbol{k_z}$ was updated at every time instant according to the following formula:

$$\boldsymbol{k_z} = k_0 + \boldsymbol{\gamma}(k_1 - k_0) \tag{3}$$

where k_1 and k_0 are the limits of range within which the stiffness parameter can vary. $\boldsymbol{\gamma}$ is a variable gain, bounded between 0 and 1 ($0 \leq \boldsymbol{\gamma} \leq 1\ \forall t$) that determines the rate of change of $\boldsymbol{k_z}$. At each time instant t, $\boldsymbol{\gamma}$ was changed according to the user's estimated force $\boldsymbol{F_h}$ and the end effector measured force $\boldsymbol{F_{ee_z}}$: $\boldsymbol{\gamma} = \boldsymbol{\gamma}(\boldsymbol{F_h}, \boldsymbol{F_{ee_z}})$. In order to obtain the desired stiffness behavior, two different $\boldsymbol{\gamma}$ profiles were used:

$$\boldsymbol{\gamma_1}(\boldsymbol{F_h}, \boldsymbol{F_{ee_z}}) = \frac{\alpha|\boldsymbol{F_{ee_z}}|}{\alpha|\boldsymbol{F_{ee_z}}| + ||\boldsymbol{F_{ee_z}}| + \boldsymbol{F_h}|} \tag{4}$$

$$\boldsymbol{\gamma_2}(\boldsymbol{F_h}, \boldsymbol{F_{ee_z}}) = \frac{\frac{1}{\alpha}|\boldsymbol{F_{ee_z}}|}{\frac{1}{\alpha}|\boldsymbol{F_{ee_z}}| + ||\boldsymbol{F_{ee_z}}| - \boldsymbol{F_h}|} \tag{5}$$

In the absence of any contact between the tooltip and the environment, the end-effector measured force was negligible ($\boldsymbol{F_{ee_z}} \approx 0$) and hence $\boldsymbol{k_z}$ remained close to k_0, resulting in a highly compliant robot. When encountering a material with a high Young's modulus, $\boldsymbol{\gamma_1}$ was maintained to keep the robot stiffness, $\boldsymbol{k_z}$, low and compliant during the procedure. In contrast, when the robot made contact with a material with a low Young's modulus, such as a vein

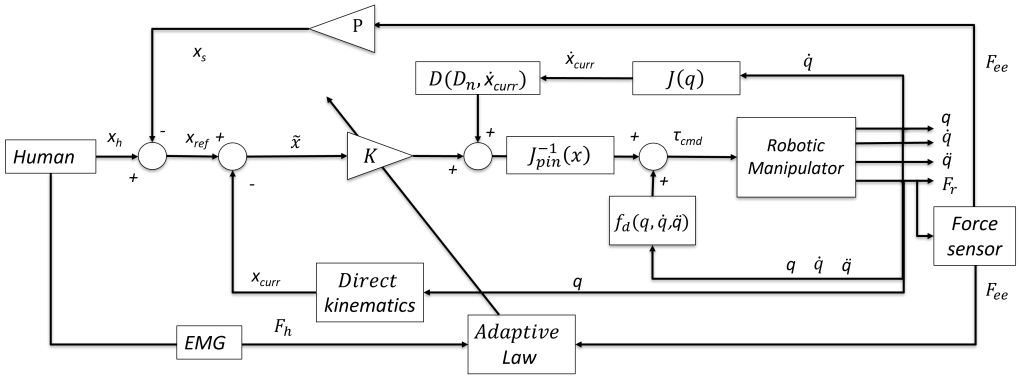

Figure 4: Scheme of the adaptive impedance control law with safety position feedback: the Cartesian reference pose $\boldsymbol{x_{ref}}$ is obtained as the difference between the position imposed by the human $\boldsymbol{x_h}$ and the safety position feedback $\boldsymbol{x_s}$, generated by multiplying $\boldsymbol{F_{ee}}$ and the gain matrix $\boldsymbol{P}$. The position error $\tilde{\boldsymbol{x}}$ is then calculated by subtracting $\boldsymbol{x_{ref}}$ and the current Cartesian pose, $\boldsymbol{x_{curr}}$. This error is multiplied by a variable stiffness matrix $\boldsymbol{K}$, controlled by an adaptive law which receives the human estimated force, $\boldsymbol{F_h}$, derived from an EMG signal and the contact force measured by the force sensor, $\boldsymbol{F_{ee}}$, as inputs. $\boldsymbol{F_{ee}}$ is measured from the force $\boldsymbol{F_r}$ that the robot exherts on the environment. The current Cartesian velocity, $\dot{\boldsymbol{x}}_{\boldsymbol{curr}}$, is used to compute the damping term $\boldsymbol{D(D_n, \dot{x}_{curr})}$, where $\boldsymbol{D_n}$ is the normalized damping matrix. The torque command in the joint space $\boldsymbol{\tau_{cmd}}$ is generated by using the Jacobian pseudo-inverse $\boldsymbol{J_{pin}^{-1}}$ and summing the inertial term $\boldsymbol{f}_d(\boldsymbol{q}, \dot{\boldsymbol{q}}, \ddot{\boldsymbol{q}})$. $\boldsymbol{q}, \dot{\boldsymbol{q}}, \ddot{\boldsymbol{q}}$ are the vectors of robot joint position, velocity, and acceleration, respectively.

or spinal cord, $\boldsymbol{\gamma_2}$ was engaged, increasing the stiffness $\boldsymbol{k_z}$ to reduce the risk of material damage. To differentiate between environments with high/low Young's modulus, a threshold, F_{tresh}, on the contact force was used. However, the condition $|\boldsymbol{F_{ee_z}}| < F_{treshold}$ was satisfied during the initial phase of contact with both material types and was insufficient to differentiate between them. The key difference between the materials was their response to forces. A material with high Young's modulus remained undamaged, while one with low Young's modulus started deforming. For this reason, the displacement ϵ was introduced as the minimum amount of deformation that occurred when in contact with a material, given the position of the end-effector ($\boldsymbol{z_{curr}}$) and the contact position ($z_{contact}$). A position treshold z_{tresh} was chosen such that $\epsilon > z_{tresh}$, and when $\boldsymbol{z_{curr}} > z_{tresh}$ and $|\boldsymbol{F_{ee_z}}| < F_{treshold}$, $\boldsymbol{\gamma_2}$ was used. In this way, the stiffness $\boldsymbol{k_z}$ was increased in order to reduce the risk of damage to the material. In Figure 5, a representation of the four possible contact situations is shown.

Additional position feedback:
In the hypothesis of an error in the surgical procedure (Fig.5, case 2b), the robotic system needs to counteract the user's action. To achieve this, the controller generated an additional position command that was proportional to the z component of $\boldsymbol{F_{ee}}$. The relation between the two signals was expressed as:

$$\boldsymbol{z}_s = \rho \boldsymbol{F_{ee_z}} \tag{6}$$

As the relation involves only one axis, the gain matrix $\boldsymbol{P}$ is reduced to the constant scalar gain ρ. In a real scenario, the surgical tool is located inside the patient body so the generated signal must be high enough to provide a solid constraint, but low enough to avoid the total loss of control of the robot.

Stability and passivity analysis:
The stability of the system was guaranteed by implementing a passivity filter. The passivity conditions obtained from the theoretical analysis were explicitly dependent on the impedance parameters. Therefore, the relation expressed in equation (3), with a generic $\boldsymbol{\gamma(t)}$ profile such that $0 \leq \boldsymbol{\gamma} \leq 1 \; \forall t$ allowed for the development of a filter that ensured passivity at every time instant. The mathematical details of the analysis and the development of the filter are discussed in Chapter 3 of the thesis.

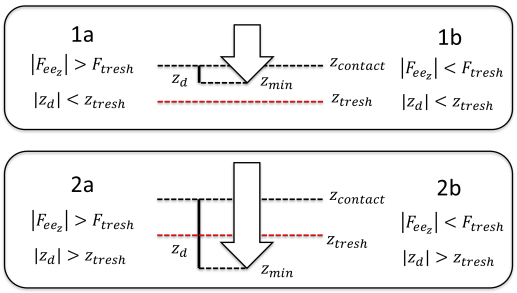

Figure 5: Scheme of the four possible contact conditions. In both cases 1a and 2a, the robot is in contact with a material with a high Young's modulus. In a real scenario, these cases correspond to the situations in which the surgeon is drilling a vertebra. Case 1b represents the first phase of the contact for both materials, while case 2b represents the contact with a material with low Young's modulus.

2.3. Experimental setup

Experimental protocol:
A User Study was conducted to compare the performance of a constant impedance hands-on control (Mode 1) with the proposed impedance control strategy (Mode 2). The goal was to demonstrate that the proposed strategy prevented the users from damaging delicate materials while allowing them to operate on a bone-like material. 10 users were asked to perform the task with the two strategies on three different materials: polyurethane (Young's modulus $\approx 1 - 10\,MPa$), PVA (Young's modulus $\approx 20 - 30\,MPa$) and a PLA vertebra phantom (Young's modulus $\approx 1 - 10GPa$) (Figure 6). The materials were placed inside a box, such that the user did not have visual feedback on the contact surface. Users were instructed to guide the robot through the object, apply a force as if attempting to perforate the material, and maintain contact for around 5 seconds. For each material, the task was repeated three times. All users gave their informed consent before participating in the study. To validate the research hypothesis, the contact force, $\boldsymbol{F_{ee_z}}$, between the robot end effector and the materials and the displacement z_d were analyzed. The displacement was computed from the contact point, $z_{contact}$, between the end-effector and the material, to the minimum point reached by the tooltip, z_{min}:

$$z_d = z_{contact} - z_{min} \tag{7}$$

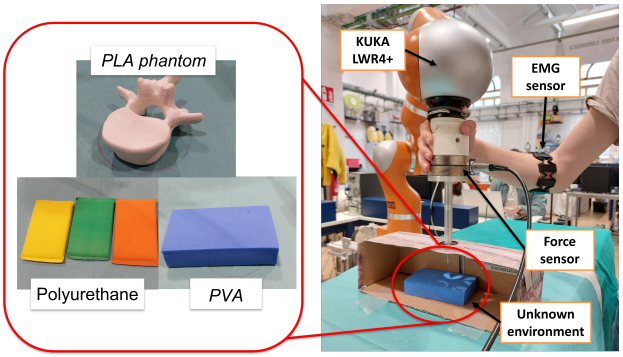

Figure 6: Experimental setup for the user study. The user guides the robot, equipped with the force sensor against different materials, placed inside a box. In Mode 2, the user is also wearing the MyoWristband on the forearm.

The average values $\hat{F}_{ee_z}$ and $\hat{z}_d$ were computed for each material $m \in [1, 2, 3]$, according to the following equations:

$$\hat{F}^m_{ee_z} = \frac{\sum_{i=1}^{r} \boldsymbol{F^i_{ee_z}}}{r} \tag{8}$$

$$\hat{z}^m_d = \frac{\sum_{i=1}^{r} |z^i_d|}{r} \tag{9}$$

where $r = 3$ are the repetitions for each user. A lower contact force $\boldsymbol{F_{ee_z}}$ and a lower displacement z_d were expected in case of contact with materials with low Young's modulus when using the proposed strategy. In the case of contact with materials with high Young's modulus, a similar performance between Mode 1 and Mode 2 was expected. As for the qualitative analysis, each user was provided with a questionnaire to fill out. The details of the questionnaire are discussed in Chapter 3 of the thesis.

System design:
The experiments were performed using the LWR4+ (KUKA) as the robotic manipulator and the MyoWristband for the EMG acquisition. The main impedance controller and the adaptive law were written in C++ and they communicate with the FRI at 100 Hz, using ROS. The sensor force and EMG processed data are acquired at 50 Hz. Regarding the impedance controller and the adaptive law, a range of $\boldsymbol{k_z}$ between $k_0 = 100\,N/m$ and $k_1 = 1000\,N/m$ was considered. Since the strategy was focused on the z-axis, the stiffness component of the other axes was kept constant. The contact force weight,

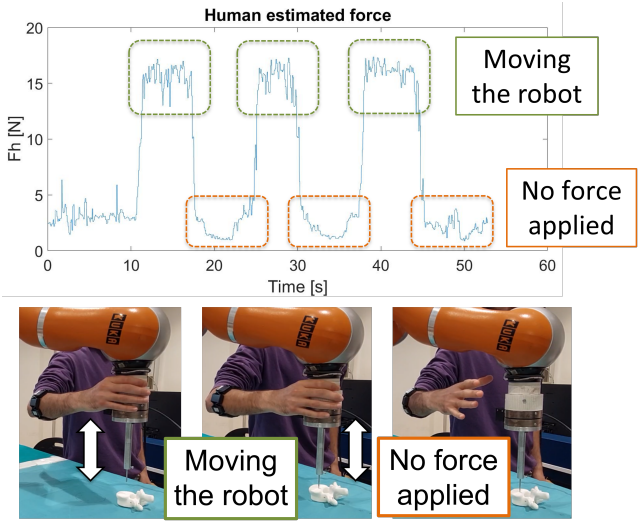

Figure 7: Human force estimated online with the LSTM trained model.

α, was chosen equal to $\alpha = 0.1$, as a result of a compromise between the two required performances. Regarding the switching logic, a force threshold, $F_{tresh} = 15\,, N$ was chosen, as a result of empirical considerations based on the reaction force caused by different materials. As displacement threshold, $z_{tresh} = 0.005\,m$, was chosen. Considering the safety feedback, a constant $\rho = 0.004\,m/N$ was chosen. In this way, the generated $\boldsymbol{z_s}$ was in the range of centimeters, which was considered enough to increase the safety of the operation, but also as small as needed to not generate unwanted behaviors on the robot.

3. Results

3.1. Force sensor

The MultiLayer Perceptron Regressor model was evaluated using the mean square error (MSE) and the R^2 score. The performance of the network is represented by an R^2 score of 0.96 and an MSE of 0.006, demonstrating its ability to accurately predict the force read by the force sensor after removing the tool gravity contribution, regardless of the end-effector orientation.

3.2. Human estimated force

The LSTM model has been validated with 20% of the collected dataset. The performance of the network is represented by an R^2 score of 0.558 and an MSE of 0.01. These results suggest that the quality of the trained network is low. Some improvements may be obtained by including, in the input data, robot joint-specific information or by considering alternative EMG sensors. In Figure 7, a plot of the human estimated force is shown. When the user applies a force on the robot and moves it, high peaks are obtained. When the user removes the hand from the robot and keeps it at rest, a low force value is obtained.

3.3. User Study

For each material, the average force and displacement among the 10 users were computed for each modality. The Wilcoxon ranksum test was used to compare the two modalities with a statistical significance assessed at 0.05. In Figure 8 the corresponding boxplots for each material are shown. The results showed that the average displacement was found significantly lower (p-value < 0.05) in Material 1 with a mean value of of $0.0074 \pm 0.0018\,m$ and $0.019 \pm 0.0068\,m$ for Mode 2 and Mode 1, respectively. Also for Material 2, a significant difference was found (p-value < 0.05) when comparing Mode 2 with Mode 1 with an average displacement of $0.0079 \pm 0.0027\,m$ and $0.0171 \pm 0.003\,m$ respectively. The results in terms of displacement show that the proposed strategy is able to recognize the type of material and prevent the user from guiding the robot through it. Furthermore, a significant difference was found in the force measured on the end-effector between Mode 1 and Mode 2 for both Material 1 and Material 2. In Material 1, Mode 2 had an average force of $-5.065 \pm 1.45\,N$, which was significantly lower than the average force of $-13.72 \pm 6.52\,N$ measured in Mode 1. Similarly, for Material 2, Mode 2 had an average force of $-5.65 \pm 2.57\,N$, which was significantly lower than the average force of $-14.79 \pm 5.15\,N$ measured in Mode 1. The lower measured force in Mode 2 when compared to Mode 1 shows that the system is able to reduce the contact force between the tooltip and the material. In this way, the risk of the material being damaged is successfully reduced. The results for Material 3 were not statistically significant, with a p-value > 0.05 for both displacement and force. This was expected since Material 3 has a high Young's modulus, and the proposed strategy was designed to keep the robot compliant during contact with such materials. Therefore, the results of the study successfully demonstrated that

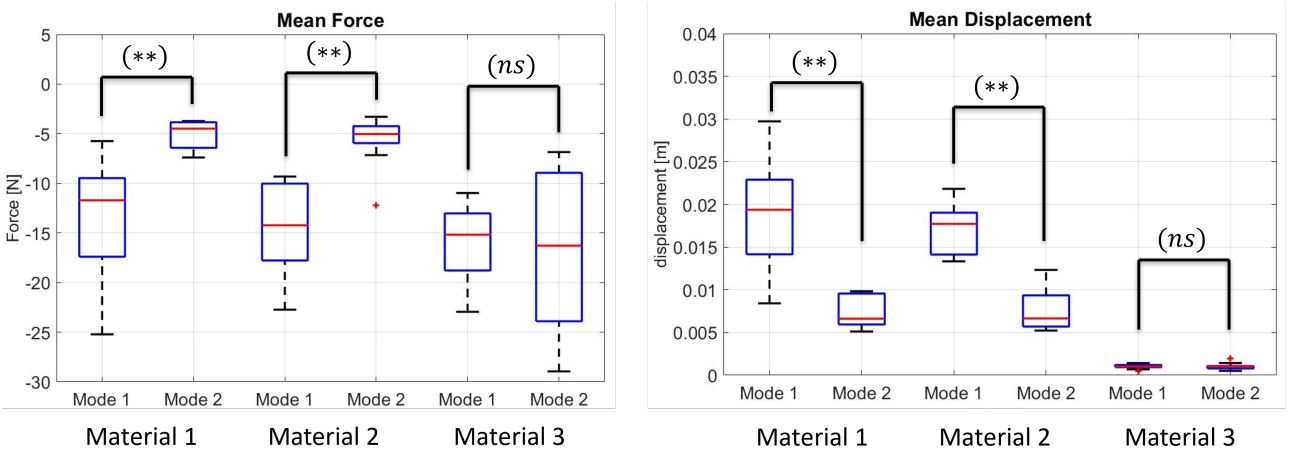

Figure 8: Comparison of the end effector contact force and average displacement between the traditional strategy (Mode 1) and the proposed strategy (Mode 2), for each material: material 1 (polyurethane), material 2 (PVA), material 3 (PLA). (**, $p < 0.01$)

the proposed strategy was effective in preventing damage to delicate materials while still allowing for effective manipulation of materials with a high Young's modulus. Regarding the qualitative analysis, the questionnaire results are discussed in Chapter 4 of the thesis.

4. Conclusions

In this study, an adaptive impedance controller was developed to change the stiffness of the robot, based on the contact force between the robot tooltip and the environment and on the human estimated force. The human force was obtained from the EMG signals of the user's arm. A safety position command was generated when contact was made with delicate materials. Results showed that the proposed strategy successfully reduces the risk of damaging such materials, in terms of contact force and displacement. The limitation of this study is the applicability in a real scenario as the analysis requires a robot equipped with an actual surgical instrument. The force sensor is subjected to measurement noise, which increases in time due to internal overheating. Finally, the different sponges used in the experiments did not accurately replicate the properties of the spinal cord and blood vessels.

References

[1] K. C. Kose, O. Bozduman, A. E. Yenigul, and Servet Igrek. Spinal osteotomies: indications, limits and pitfalls. *EFORT Open Reviews*, 2(3):73 – 82, 2017.

[2] Oussama Khatib Bruno Siciliano, editor. *Springer Handbook of Robotics*. Springer-Verlag Berlin Heidelberg, 2008.

[3] Elisa Beretta, Elena De Momi, Ferdinando Rodriguez y Baena, and Giancarlo Ferrigno. Adaptive hands-on control for reaching and targeting tasks in surgery. *International Journal of Advanced Robotic Systems*, 12(5):50, 2015.

[4] Hsieh-Yu Li, Theshani N., S. Alex X., and U-Xuan T. Towards a compliant and accurate cooperative micromanipulator using variable admittance control. In *2018 3rd International Conference on Advanced Robotics and Mechatronics (ICARM)*, pages 230–235, 2018.

[5] B. Bayle M. Bednarczyk, H. Omran. Emg-based variable impedance control with passivity guarantees for collaborative robotics. *IEEE Robotics and automation letters*, 7:4307–4312, 2022.

[6] Hang Su, Wen Qi, Zhijun Li, Ziyang Chen, Giancarlo Ferrigno, and Elena De Momi. Deep neural network approach in emg-based force estimation for human–robot interaction. *IEEE Transactions on Artificial Intelligence*, 2(5):404–412, 2021.